Journal of Catalysis 259 (2008) 260–268

Contents lists available at ScienceDirect

Journal of Catalysis

www.elsevier.com/locate/jcat

Low temperature hydrogenation of benzene and cyclohexene: A comparative study between γ-Al_2O_3 supported PtCo and PtNi bimetallic catalysts

Shuliang Lu [a,c], William W. Lonergan [b], Jeffery P. Bosco [b], Songrui Wang [a], Yuexiang Zhu [a,*], Youchang Xie [a], Jingguang G. Chen [b,*]

[a] Beijing National Laboratory for Molecular Sciences, State Key Laboratory for Structural Chemistry of Unstable and Stable Species, College of Chemistry and Molecular Engineering, Peking University, Beijing 100871, China
[b] Department of Chemical Engineering, Center for Catalytic Science and Technology (CCST), University of Delaware, Newark, DE 19716, USA
[c] Institute of Theoretical and Computational Chemistry and Center for Computational Science and Engineering, Peking University, Beijing 100871, China

ARTICLE INFO

Article history:
Received 9 July 2008
Revised 27 August 2008
Accepted 30 August 2008
Available online 27 September 2008

Keywords:
Hydrogenation
Benzene
Cyclohexene
Pt–Co
Pt–Ni
γ-Al_2O_3
Bimetallic catalysts
FTIR
EXAFS

ABSTRACT

Supported PtCo and PtNi bimetallic and Co, Ni, Pt monometallic catalysts were prepared by impregnation method on γ-Al_2O_3 and evaluated for the hydrogenation of benzene and cyclohexene at low temperatures (273–343 K) and atmospheric pressure. Results from batch reactor studies with Fourier transform infrared spectroscopy (FTIR) and flow reactor studies both showed that PtCo bimetallic catalysts exhibited significantly higher activity than PtNi and monometallic Co, Ni, and Pt catalysts for benzene hydrogenation, while PtNi catalysts showed higher activity for cyclohexene hydrogenation. Results from H_2 chemisorption and H_2-temperature-programmed reduction (H_2-TPR) studies showed that a small amount of Pt addition could increase the chemisorption capacity and make the reduction of Co or Ni much easier, especially for Co-based catalysts. Extended X-ray absorption fine structure (EXAFS) results confirmed the formation of Pt–Co and Pt–Ni bimetallic bonds in the PtCo and PtNi bimetallic catalysts, supporting the argument from previous surface science and theoretical predictions that these two bimetallic catalysts would have higher hydrogenation activity than the corresponding monometallic catalysts.

1. Introduction

The hydrogenation of benzene to cyclohexane is of significant importance in the petroleum industry and for environmental protection. The process of benzene hydrogenation has been utilized commercially for the production of cyclohexane, which is one of the key intermediates in the synthesis of Nylon-6 and Nylon-66 [1]. Recently, the hydrogenation of benzene has attracted renewed attention for the reduction of the aromatic content in petroleum products, especially in gasoline and diesel [2]. Additionally, kinetic and thermodynamic results show that polyaromatics are more easily reduced than benzene under moderate conditions [2]. Thus, the development of active catalysts for benzene hydrogenation is of both fundamental and practical importance.

Catalysts based on group VIII metals, such as Ni [3–13], Fe [14–16], Pt [17,18], Pd [19,20], Ru [21–23] and Co [24–29], have been used for the hydrogenation of benzene. Among them, Ni- and Pt-based catalysts have been extensively studied and are already used in commercial processes. Ru-based catalysts are often used for partial hydrogenation of benzene to cyclohexene [21–23]. Some new catalytic materials, such as amorphous metal alloys [30] and ionic-liquid-like copolymer stabilized nanocatalysts in ionic liquids [31], have also been used for benzene hydrogenation. Although supported cobalt catalysts have been widely used in Fischer–Tropsch synthesis [32,33], relatively few studies have been reported concerning benzene hydrogenation over Co-based catalysts.

It is well known that bimetallic catalysts often show properties that are distinctly different from those of the corresponding monometallic catalysts [34–38], including the enhancement of hydrogenation activities. Many investigations combining fundamental surface science studies and theoretical calculations have been performed with the goal of correlating electronic properties of bimetallic surfaces with catalytic properties [36–47]. More recently, it has been demonstrated that Ni/Pt(111) and Co/Pt(111) bimetallic surfaces [32,43,47], with Ni or Co atoms residing in the subsurface region in Pt(111), designated as Pt–Ni–Pt(111) or Pt–Co–Pt(111), showed much higher activity for the hydrogenation of cyclohexene than the corresponding monometallic surfaces. The novel low-temperature hydrogenation pathway on the bimetallic surfaces has been correlated to the modification of the electronic properties due to the formation of the subsurface bimetallic structures [47]. In

* Corresponding authors.
E-mail addresses: zhuyx@pku.edu.cn (Y. Zhu), jgchen@udel.edu (J.G. Chen).

0021-9517/$ – see front matter
doi:10.1016/j.jcat.2008.08.016

Table 1
Catalyst compositions and H_2 chemisorption results.

Catalyst	Metal content (wt%)			H_2 uptake (μmols/g catalyst)	Dispersion from chemisorption (%)
	Co	Ni	Pt		
10%Co/γ-Al_2O_3	10			14.4	1.7
10%Ni/γ-Al_2O_3		10		27.0	3.2
1.2%Pt–10%Co/γ-Al_2O_3	10		1.2	30.6	3.3
1.2%Pt–10%Ni/γ-Al_2O_3		10	1.2	75.2	7.5
1.2%Pt/γ-Al_2O_3			1.2	7.2	46
30%Co/γ-Al_2O_3	30			24.9	1.0
30%Ni/γ-Al_2O_3		30		105	4.2
1.2%Pt–30%Co/γ-Al_2O_3	30		1.2	50.0	2.0
1.2%Pt–30%Ni/γ-Al_2O_3		30	1.2	118	4.6

these surface science experiments the Pt–Ni–Pt(111) and Pt–Co–Pt(111) subsurface structures were prepared by depositing Ni and Co on Pt(111) at 600 K, with the subsurface structures being stable either in vacuum or with adsorbed atomic hydrogen [47].

The main objective of the present work is to extend the surface science results to γ-Al_2O_3 supported PtCo, PtNi bimetallic catalysts and Co, Ni, Pt monometallic catalysts prepared by the impregnation method. In order to maximize the formation of the Pt–Ni and Pt–Co bimetallic bonds, the atomic ratios of Ni/Pt and Co/Pt in the current work are chosen to be significantly higher than previous studies [48]. The hydrogenation of cyclohexene on the supported catalysts was used as a probe reaction to demonstrate the enhanced hydrogenation activity toward the C=C bond on the bimetallic catalysts, as predicted from the surface science studies [47]. The hydrogenation of benzene was then investigated on the bimetallic catalysts at a relatively low temperature (343 K) and atmospheric pressure. The supported PtCo bimetallic catalysts exhibited much better performance than the others for benzene hydrogenation in both batch and flow reactor studies. On the other hand, for cyclohexene hydrogenation PtNi bimetallic catalysts showed higher activity than PtCo catalysts, consistent with predictions from surface science studies [47]. Furthermore, H_2 chemisorption, H_2-TPR and EXAFS were used to characterize the bimetallic catalysts and to determine the possible origin of the enhanced hydrogenation activities of the bimetallic catalysts.

2. Experimental

2.1. Catalyst preparation

All of the catalysts were prepared by the impregnation method. The support precursor (pseudo-boehmite) was first calcined at 823 K for 5 h before impregnation to achieve the γ-Al_2O_3 structure, with a BET specific surface area of 228 m^2/g and a total pore volume of 0.44 cm^3/g. The $Co(NO_3)_2{\cdot}6H_2O$ (A.R.) precursor was dissolved in deionized water and impregnated into the support to produce a catalyst of 10 wt% Co over γ-Al_2O_3. The 1.2wt%Pt–10wt%Co/γ-Al_2O_3 bimetallic catalyst was prepared by co-impregnation using $Pt(NH_3)_4(NO_3)_2$ (Acrös Organics, 99%) and $Co(NO_3)_2{\cdot}6H_2O$ (A.R.). After the impregnation, the catalysts were dried at 383 K for 12 h and then calcined in air at 773 K for 4 h. The 10wt%Ni/γ-Al_2O_3 and 1.2wt%Pt–10wt%Ni/γ-Al_2O_3 catalysts were prepared using the same method and using $Ni(NO_3)_2{\cdot}6H_2O$ (A.R.) as the nickel precursor. The catalysts with 30 wt% Co or Ni loading were also prepared to make comparisons with the catalysts with 10 wt% Co or Ni loading. The compositions of all the catalysts are summarized in Table 1.

2.2. Catalyst characterization

2.2.1. H_2-temperature-programmed reduction (H_2-TPR)

TPR experiments were performed to determine the reduction behavior of the catalysts. The experiments were carried out in a U-shaped tubular quartz reactor heated by an electric furnace. 0.010 g of calcined catalyst (60–80 mesh) was exposed to a reducing gas consisting of 5.0 vol% H_2 in Ar with a temperature ramp from 298 K to 1173 K at 10 K/min. The amount of hydrogen consumption was detected by a thermal conductivity detector (TCD).

2.2.2. H_2 chemisorption

H_2 chemisorption experiments were carried out using the Micromeritics ASAP2010C instrument. A volumetric static method was used for H_2 chemisorption. Prior to H_2 chemisorption, the catalysts (~0.10 g, 60–80 mesh) were reduced by H_2 at 723 K for 2 h and then evacuated at 723 K for 3 h, and 308 K for 1 h to desorb any hydrogen from the catalysts. The H_2 adsorption isotherms were then measured to determine the H_2 uptake at 308 K in the pressure range of 50–450 Torr. An initial H_2 adsorption isotherm was achieved to measure the total amount of adsorbed H_2 (chemisorbed and physisorbed). The catalyst was then outgassed in the measurement unit and then a second H_2 adsorption isotherm was measured to evaluate the amount of physisorbed H_2. The total chemisorbed amount of H_2 was deduced by subtracting the second isotherm from the first one and extrapolating the nearly horizontal difference curve to the uptake axis.

The uptake of H_2 on the catalysts is compared in Table 1. The calculation of metal dispersion was based on H_2 chemisorption and assumed stoichiometry of $M{:}H_2 = 2{:}1$ (M=Pt, Co, Ni). Because of the large amount of Ni and Co loadings in the catalysts, the dispersion values on these catalysts are not very meaningful and are listed in Table 1 to only provide a relative ranking of metal dispersion. However, the amount of adsorbed hydrogen provides a quantitative comparison of the number of active sites among the various monometallic and bimetallic catalysts.

2.2.3. Extended X-ray absorption fine structure (EXAFS)

EXAFS measurements of the Pt L_{III}-edge were performed in order to confirm the presence of the Pt–Co and Pt–Ni bimetallic bonds. The EXAFS experiments for the 1.2%Pt–10%Co/γ-Al_2O_3 and 1.2%Pt–10%Ni/γ-Al_2O_3 catalysts were conducted on the X18B and X19A beamlines, respectively, at the National Synchrotron Light Source (NSLS), Brookhaven National Laboratory. EXAFS samples were prepared by pressing the powder catalyst into pellets using a force of approximately 3 tons per cm^2. The mass of the pellets was chosen so that the samples would have a thickness on the order of two absorption lengths to optimize the signal to noise ratio. Samples were then placed into an EXAFS cell that allowed for *in situ* reduction and for simultaneous collection of both transmission and fluorescence signals. The catalysts were heated to 723 K at a rate of 14 K/min under a diluted hydrogen flow (5% H_2 in He, 40 cc/min), and held at 723 K for 1 h before cooling to room temperature. EXAFS measurements of the Pt L_{III}-edge were collected at room temperature using a double crystal Si(111) monochromator. The incident and transmitted X-ray signals were measured with ionization chambers and a germanium detector was used to collect

the fluorescence signal. The edge energies of the EXAFS spectra were calibrated to the edge of a Pt foil collected in transmission mode.

The EXAFS collection was collected in three energy regions: the pre-edge region from −150 to −25 eV before the edge, the near-edge region ranging from −25 eV before the edge to 40 eV past the edge, and the post-edge region from 40 eV to 18 k (approximately 1450 eV) past the edge. The respective step sizes in each of these regions were 5 eV, 0.5 eV, and 0.05 k (approximately 3 eV). Similarly the integration times varied for each region, and the times used were 1 s, 2 s, and 2 s, respectively.

The X-ray absorption data from the fluorescence signal was analyzed using the IFFEFIT 1.2.10 data analysis package (Athena, Artemis, Atoms, and FEFF6) [49,50]. Data reduction consisted of aligning the scans to the foil standard and deglitching each scan when necessary. The multiple scans collected for each edge were then merged to reduce experimental error and then the AUTOBK algorithm in Athena was used to remove the isolated-atom background function from the EXAFS data. The EXAFS signal was then Fourier-transformed into R-space and Artemis was used to obtain local structural information for the first coordination shell. The Pt L_{III}-edges were modeled by including both Pt–Pt and Pt–3d (Co or Ni) contributions in the theoretical EXAFS generated using FEFF6. The Pt–Pt theoretical photoelectron scattering-path amplitudes and phases were calculated for the bulk Pt fcc structure. Pt–3d contributions were modeled in FEFF6 by using the same Pt fcc structure with the exception that the Pt atoms in the first nearest-neighbor shell were replaced with the appropriate 3d metal atom. The seven variables used in the fitting procedure were the coordination numbers of Pt–Pt and Pt–Ni bonds, two corrections to the model interatomic distances, two EXAFS Debye–Waller factors (mean-square deviations in interatomic distances), and the correction to the photoelectron energy. By fitting the Pt reference foil, the passive electron reduction factor, $S_0^2 = 0.85$ was determined, and this value was held fixed in the analysis of the bimetallic catalysts.

2.3. Catalytic activity tests

2.3.1. Flow reactor study

The hydrogenation of benzene was carried out in a quartz glass reactor under atmospheric pressure at 343 K. The flow of benzene, controlled by a micro-syringe pump with a flow rate of 5.6 mmol/h, was carried by H_2 with a gas flow rate of 10 ml/min and N_2 with a gas flow rate of 40 ml/min. For each experiment, 0.10 g of unreduced catalyst (60–80 mesh) was loaded into the flow reactor. Before the reaction, the catalyst was reduced under hydrogen (20 ml/min) and nitrogen (20 ml/min) mixture at 723 K for 1 h. The product streams were analyzed by online gas chromatography equipped with a flame ionization detector (FID).

In order to correlate with previous surface science studies [47], the hydrogenation of cyclohexene was also used as a probe reaction in the same flow reactor. For each experiment, 0.040 g of unreduced catalyst was used for the catalytic evaluation under atmospheric pressure at 273 K. After the reduction of catalyst using the conditions described above, cyclohexene was injected by a micro-syringe pump at a flow rate of 4.9 mmol/h and was carried by H_2 with a gas flow rate of 3 ml/min and N_2 with a gas flow rate of 47 ml/min.

2.3.2. Batch reactor study using FTIR

Fourier transform infrared (FTIR) spectroscopy was employed to monitor the concentrations of individual reactants and products during the hydrogenation of cyclohexene and benzene within a batch reactor system. The stainless steel IR cell, fitted with infrared-transparent BaF_2 windows and capable of base pressures below 1×10^{-6} Torr, allowed for *in situ* reduction of samples and spectroscopic measurements of either surface species or gas-phase products before, during, and after reduction/reaction. All spectra were recorded with 4 cm^{-1} resolution using a Nicolet-470 FTIR spectrometer equipped with a MCT-A (mercury cadmium telluride) detector.

Each catalyst was supported within the reactor using a tungsten mesh (1 × 2.4 cm, 100 mesh, 0.001 in wire diameter, Alfa Aesar) connected to a nickel mounting bracket at the end of a z-translating manipulator and feedthrough. Catalyst powders were pressed in direct contact with the mesh using a force of 3 tons per cm^2. Also attached to the mesh was a K-type thermocouple to monitor the temperature of the catalyst during reduction. The feedthrough provided connections for the thermocouple and leads for resistive heating of the catalyst pellet through the supporting tungsten mesh. The gases and liquid vapors necessary for reduction, venting, adsorption, or hydrogenation reactions were admitted into the IR cell through a connecting gas manifold that was also maintained under high vacuum.

For all of the hydrogenation experiments, ∼25 mg of alumina-supported catalyst was employed. After connecting a fresh catalyst to the manipulator arm, the cell was first evacuated to a pressure below 1×10^{-6} Torr for a minimum of 60 min in order to remove water and other impurities. The catalyst was then reduced at 723 K in 30 Torr of hydrogen for 30 min followed by evacuation and a high temperature flash (723 K) to remove any surface species generated during reduction. This reduction process was repeated three times before performing the FTIR experiments. During hydrogenation reactions, the gas-phase reactants and products were monitored by recording IR spectra (32 scans) every 30 s. The purity of cyclohexene and benzene vapors was verified *in situ* prior to any experimentation by comparing the IR spectrum with the standard reference reported in literature [51]. Before initiation of a reaction, IR spectra of the reactor cell under vacuum were collected for 10 min in order to determine an appropriate baseline. During this collection period, reactant species were premixed at room temperature within the gas manifold. For the hydrogenation of cyclohexene, hydrogen gas and cyclohexene vapor were mixed at a partial pressure ratio of 2:1, while for the benzene hydrogenation experiments the ratio of hydrogen to benzene was 6:1. To initiate the reaction, the gas/vapor mixture was rapidly dosed into the batch cell with the catalyst already heated to a chosen reaction temperature. The hydrogenation reactions proceeded at catalyst temperatures of 303 and 343 K and initial pressures of ∼5.5 and ∼8.0 Torr for cyclohexene and benzene, respectively.

The concentrations of the three main gas-phase species during the hydrogenation reactions (cyclohexene, cyclohexane, and benzene) were estimated using the intensities of the characteristic vibrational modes at 1139 cm^{-1} (ωCH_2 rock), 1458 cm^{-1} ($-CH_2$ deformation), and 1810 cm^{-1} (overtone of the C–C stretching mode at 993 cm^{-1}), respectively, as described in detail previously for the disproportionation (self-hydrogenation) reaction of cyclohexene [48].

3. Results

3.1. H_2-temperature-programmed reduction (H_2-TPR)

The reducibility of the calcined catalysts was studied by TPR and the reduction profiles are shown in Fig. 1. For the pure cobalt oxide (Co_3O_4), there were two major peaks ascribed to the successive reduction of bulk Co_3O_4 to CoO to Co [52]. The γ-Al_2O_3 supported cobalt catalysts show a much broader reduction temperature range because of the strong interaction between Co and the alumina support [32,33]. The reduction process has been related to the following steps: Co_3O_4 clusters to CoO, bulk-like CoO to Co, and Co_xO_y–Al_2O_3 to Co metal [32]. As shown in Fig. 1,

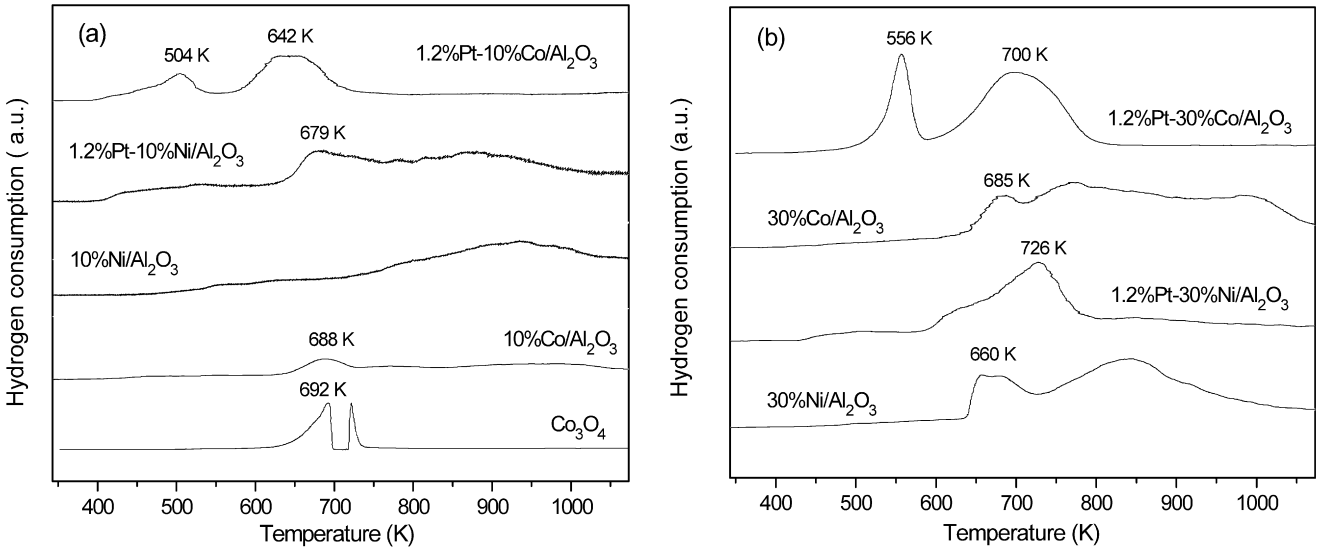

Fig. 1. TPR profiles of the calcined catalysts: (a) catalysts with 10% Co(Ni) loading, (b) catalysts with 30% Co(Ni) loading.

supported PtCo and PtNi bimetallic catalysts could be reduced at a much lower temperature than the corresponding monometallic catalysts and the reduction temperature range became narrower. For example, the reduction temperature of the first step decreased from approximately 688 K for 10%Co/γ–Al_2O_3 to 504 K for the 1.2%Pt–10%Co/γ-Al_2O_3 bimetallic catalyst. The presence of Pt in the Pt–Co catalysts appears to promote the reduction of cobalt oxides through hydrogen spillover. Pt can be reduced at lower temperatures than Co, therefore hydrogen that dissociates on the surface of Pt could migrate to the surface of Co_3O_4 and support, resulting in Co being reduced at much lower temperatures in the bimetallic catalysts.

In comparison, for supported PtNi bimetallic catalysts the effect of Pt addition was not as effective as that of PtCo bimetallic catalysts. There was still a broad reduction temperature range for the 1.2%Pt–10%Ni/γ-Al_2O_3 catalyst, although the onset of the reduction temperature was decreased as compared to 10%Ni/γ-Al_2O_3. Fig. 1b shows the TPR results of catalysts with higher 30% Co or Ni loadings. The reduction profiles are in general similar to those of the corresponding 10% catalysts, although the hydrogen consumption was higher in Fig. 3b due to higher Co and Ni loadings.

3.2. Extended X-ray absorption fine structure (EXAFS)

EXAFS measurements were performed on the 1.2%Pt–10%Co/γ-Al_2O_3 and 1.2%Pt–10%Ni/γ-Al_2O_3 catalysts in order to verify the formation of bimetallic bonds. In the fitting of the Pt L_{III}-edges, the k-ranges were selected so as to exclude regions of noise at high-k. The chosen k-ranges were between 2 and 15 for the PtCo catalyst, and between 2.5 and 12 for the PtNi catalyst. The spectra for both catalysts were k^2-weighted in order to obtain the best fits. In Fourier-transforming the spectra, a Hanning window with a sill width of 2 $Å^{-1}$ was used. The resulting transformations into R-space and the fits obtained in Artemis are shown in Fig. 2. The fits shown in Fig. 2 are for the first coordination shell only, and the fitting results are presented in Table 2.

For the bulk metals, the Co–Co, Ni–Ni and Pt–Pt first nearest neighbor distances are 2.506, 2.492 and 2.774 Å, respectively. If the Co, Ni and Pt were to segregate into monometallic nanoparticles, their first nearest neighbor distance would be similar or slightly smaller than that in the bulk, with the latter being due to the particle size effect on the interatomic distance. In the case of alloying, the nearest neighbor distance should be an intermediate

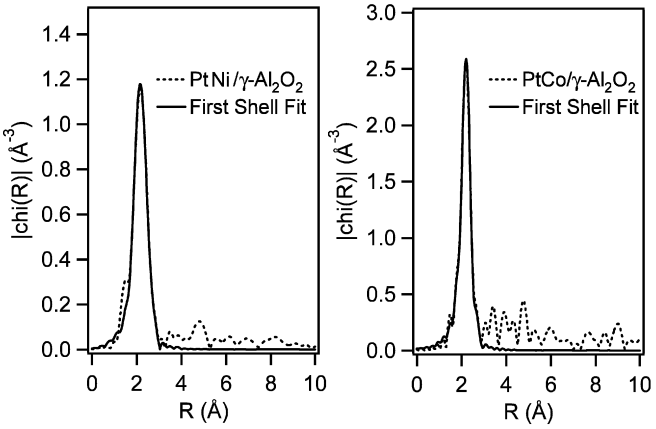

Fig. 2. Fourier-transformed k^2-weighted EXAFS function ($\chi(k)$) of Pt L_{III}-edge of 1.2%Pt–10%Ni/γ-Al_2O_3 and 1.2%Pt–10%Co/γ-Al_2O_3, filtered (dashed) and fitted (solid) EXAFS curves.

Table 2
Summary of Pt L_{III}-edge fitting for 1.2%Pt–10%Co/γ-Al_2O_3 and 1.2%Pt–10%Ni/γ-Al_2O_3.

Catalyst	1.2%Pt–10%Co/γ-Al_2O_3	1.2%Pt–10%Ni/γ-Al_2O_3
N(Pt–Pt)	0.6 ± 1.2	1.6 ± 1.2
N(Pt–3d)	6.0 ± 0.7	4.6 ± 0.8
R(Pt–Pt), Å	2.70 ± 0.03	2.65 ± 0.02
R(Pt–3d), Å	2.55 ± 0.04	2.53 ± 0.01
σ^2(Pt–Pt), Å^2	0.004 ± 0.006	0.004 ± 0.004
σ^2(Pt–3d), Å^2	0.005 ± 0.001	0.008 ± 0.001

value between the two monometallic distances. From the results in Table 2, the Pt–Co and Pt–Ni distances are determined to be 2.55 ± 0.04 and 2.53 ± 0.01, respectively. These distances are between the bulk 3d–3d and Pt–Pt distances, consistent with the presence of bimetallic bonds.

The Pt–Co and Pt–Ni coordination numbers were found to be 6.0 ± 0.7 and 4.6 ± 0.8, respectively, while the Pt–Pt coordination numbers were found to be smaller in both catalysts. This indicates that there are many more Pt–3d bonds than Pt–Pt bonds, suggesting that most Pt atoms are primarily coordinated with 3d atoms, which is expected due to the large 3d/Pt atomic ratios of the PtCo and PtNi catalysts.

3.3. Flow reactor study using GC

The hydrogenation of cyclohexene, a model hydrogenation reaction that was used previously on single crystal bimetallic surfaces [42,47], was performed in the current study to test the catalytic activity for C=C bond hydrogenation. Cyclohexane was the only reaction product detected by online gas chromatography. Fig. 3 shows the conversion of cyclohexene over 1.2%Pt–10%Co/γ-Al_2O_3, 1.2%Pt–10%Ni/γ-Al_2O_3 and 1.2%Pt/γ-Al_2O_3 catalysts at 273 K. The hydrogenation of cyclohexene over 10%Co/γ-Al_2O_3 and 10%Ni/γ-Al_2O_3 catalysts was also tested and the catalytic activity was nearly zero, which was not shown in Fig. 3. It was found that the PtNi bimetallic catalyst showed better performance than PtCo. This was consistent with the H_2 chemisorption results, which indicated that PtNi catalyst had more metallic active sites. More importantly, the results in Fig. 3 clearly showed that the PtNi and PtCo bimetallic catalysts were more active than Pt, in agreement with previous studies on single crystal surfaces [47]. After establishing the higher hydrogenation activity for cyclohexene, the bimetallic catalysts were evaluated for benzene hydrogenation at 343 K and atmospheric pressure, which were rather moderate reaction conditions for benzene hydrogenation. Cyclohexane was the only reaction product detected by online gas chromatography. As shown in Fig. 4a, the conversion of benzene was nearly zero for γ-Al_2O_3 supported 10% Co and 10% Ni monometallic catalysts, about 5% for 1.2% Pt, and about 4% for 1.2%Pt–10%Ni. In comparison, the 1.2%Pt–10%Co catalyst showed a much higher conversion of ~30%. When Co or Ni loading increased to 30% in the catalysts (Fig. 4b), the conversion of benzene was still low for the 30%Ni and 1.2%Pt–30%Ni catalysts, while for the 30% Co and 1.2%Pt–30%Co catalysts the conversion increased compared to the corresponding catalysts with 10% Co loading, which was partially attributed to more active sites for benzene hydrogenation (Fig. 4b). In particular, for the 1.2%Pt–30%Co/γ-Al_2O_3 catalyst, the initial conversion of benzene increased to ~50%. In summary, PtCo bimetallic catalysts showed much higher activities than Co, Ni, Pt monometallic and PtNi bimetallic catalysts for benzene hydrogenation. PtNi and Pt had nearly the same relatively low activities, indicating that Ni was not good for benzene hydrogenation at low temperatures.

The apparent activation barriers for benzene hydrogenation reactions were estimated over several monometallic and bimetallic catalysts, as shown in Fig. 5. The most significant difference was that Co-based catalysts had lower activation barriers than Ni-based catalysts for benzene hydrogenation.

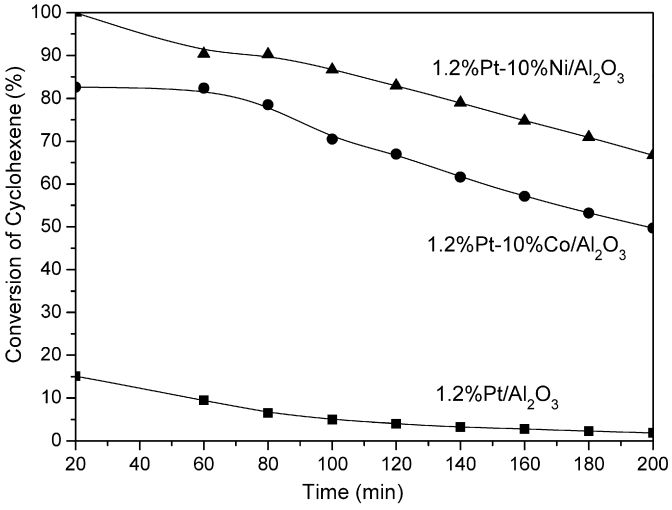

Fig. 3. Flow reactor study of cyclohexene hydrogenation at 273 K over 1.2%Pt–10%Co/γ-Al_2O_3, 1.2%Pt–10%Ni/γ-Al_2O_3 and 1.2%Pt/γ-Al_2O_3 catalysts. Experiment conditions: H_2: cyclohexene = 1.5:1, catalyst amount: 40 mg.

3.4. Batch reactor study using FTIR

The rates of cyclohexene and benzene hydrogenation were evaluated for the PtNi and PtCo bimetallic and Pt monometallic catalysts using a batch reactor. Fig. 6 displays the consumption of cyclohexene and production of cyclohexane as a function of reaction time for each of the catalysts. It was observed that the rate of cyclohexane production over the bimetallic catalysts was greater than that of the monometallic Pt catalyst and that the PtNi catalyst was more active than PtCo. The experimental results were modeled using a classic Langmuir–Hinshelwood mechanism, assuming the rate-determining step (RDS) for the hydrogenation of cyclohexene is the addition of the first hydrogen atom. The solid lines in Fig. 6 are those obtained from the following equation for the rate of production of cyclohexane and similar expression for cyclohexene consumption using the classic Langmuir–Hinshelwood model:

$$r_{C_6H_{12}} = -r_{C_6H_{10}} = \frac{k_1 K_C C_{C_6H_{10}} \sqrt{K_{H_2} C_{H_2}}}{(1 + K_C C_{C_6H_{10}} + \sqrt{K_{H_2} C_{H_2}})^2}. \quad (1)$$

Within the rate expression, k_1 represents the rate constant for the addition of the first hydrogen and K_C and K_{H_2} are equilib-

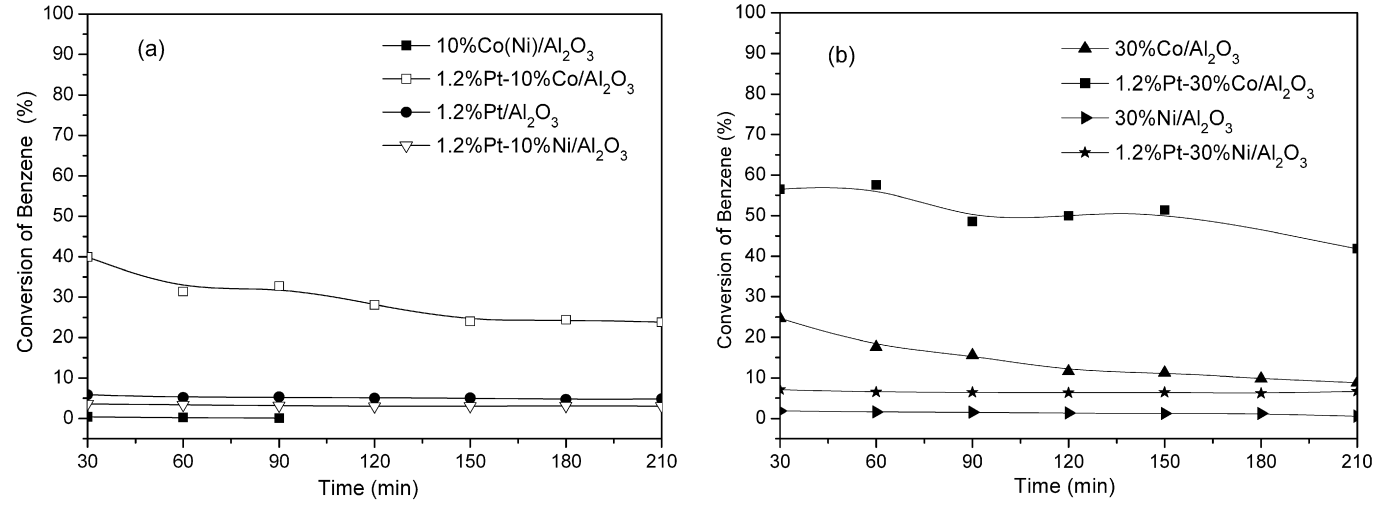

Fig. 4. Flow reactor study of benzene hydrogenation at 343 K: (a) catalysts with 10% Co(Ni) loading, (b) catalysts with 30% Co(Ni) loading. Experiment conditions: H_2: benzene = 5:1, catalyst amount: 100 mg.

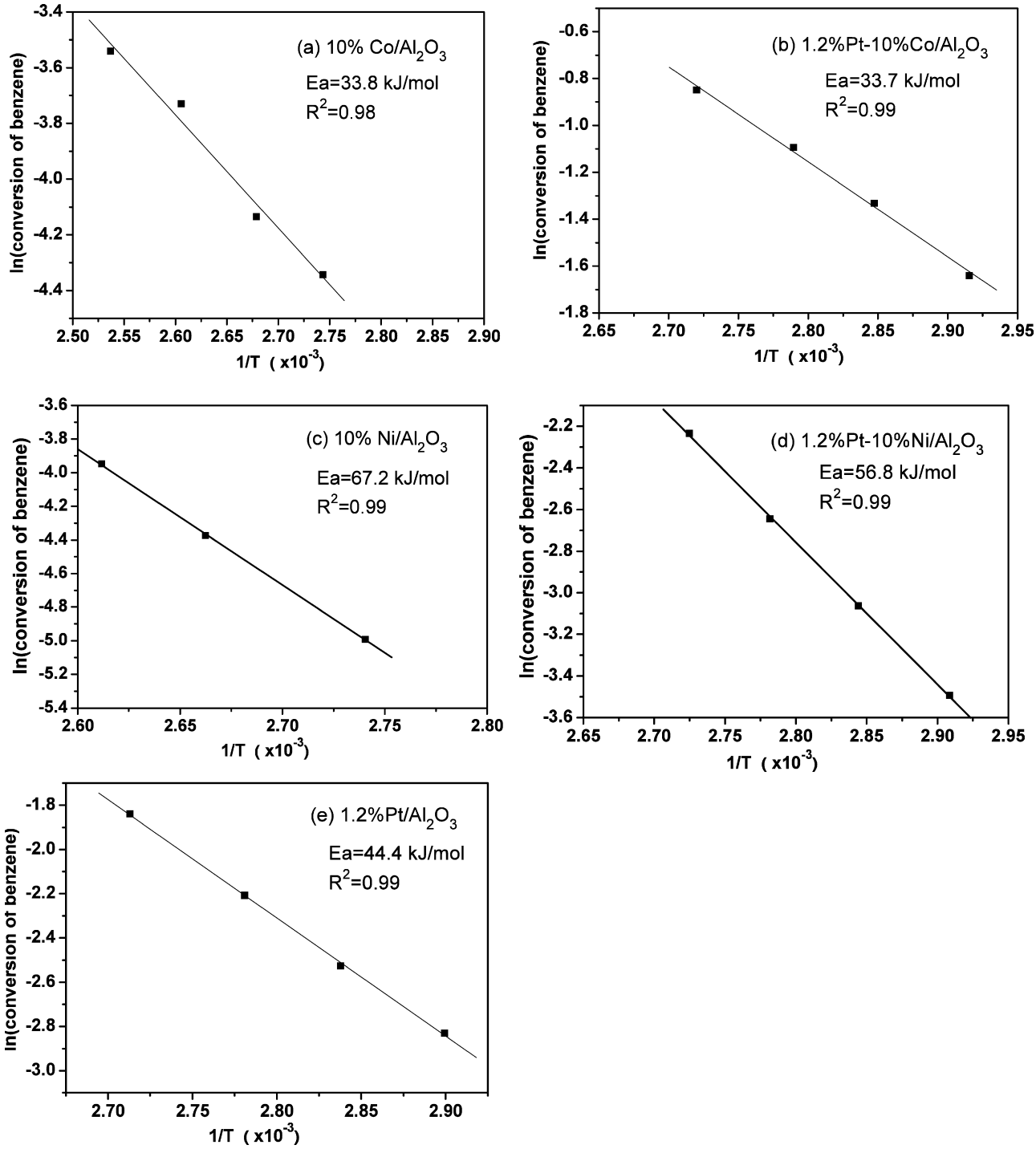

Fig. 5. Estimation of the apparent activation energy for benzene hydrogenation from flow reactor studies: (a) 10%Co/γ-Al_2O_3, (b) 1.2%Pt–10%Co/γ-Al_2O_3, (c) 10%Ni/γ-Al_2O_3, (d) 1.2%Pt–10%Ni/γ-Al_2O_3, (e) 1.2%Pt/γ-Al_2O_3.

rium constants for the adsorption/desorption of gaseous cyclohexene and hydrogen species to and from the catalyst surface sites. During the fitting, the equilibrium constant K_{H_2} was held at a value of 0.56 $cm^3\,mol^{-1}$ based on [53]. The fitted values for rate constant, k_1, are summarized in Table 3. In summary, the catalytic activity of the three catalysts shows the following trend: 1.2%Pt–10%Ni/γ-Al_2O_3 > 1.2%Pt–10%Co/γ-Al_2O_3 > 1.2%Pt/γ-Al_2O_3, which is consistent with the trend from flow reactor studies shown earlier in Fig. 3.

It should be noted that for the PtNi and PtCo supported catalysts, there was a small amount of benzene production observed (data not shown) at the start of the cyclohexene hydrogenation reaction followed by its slow disappearance. Benzene production was likely due to the dehydrogenation or disproportionation (i.e. self-hydrogenation) of cyclohexene in parallel with the hydrogenation reaction. This argument is in agreement with previous studies on cyclohexene self-hydrogenation over similar catalysts [48]. Benzene production was not observed to any noticeable extent over the Pt monometallic catalyst.

The rates of cyclohexane production and benzene consumption for the hydrogenation of benzene over the same three catalysts are displayed in Fig. 7. It was determined that the PtCo catalyst was

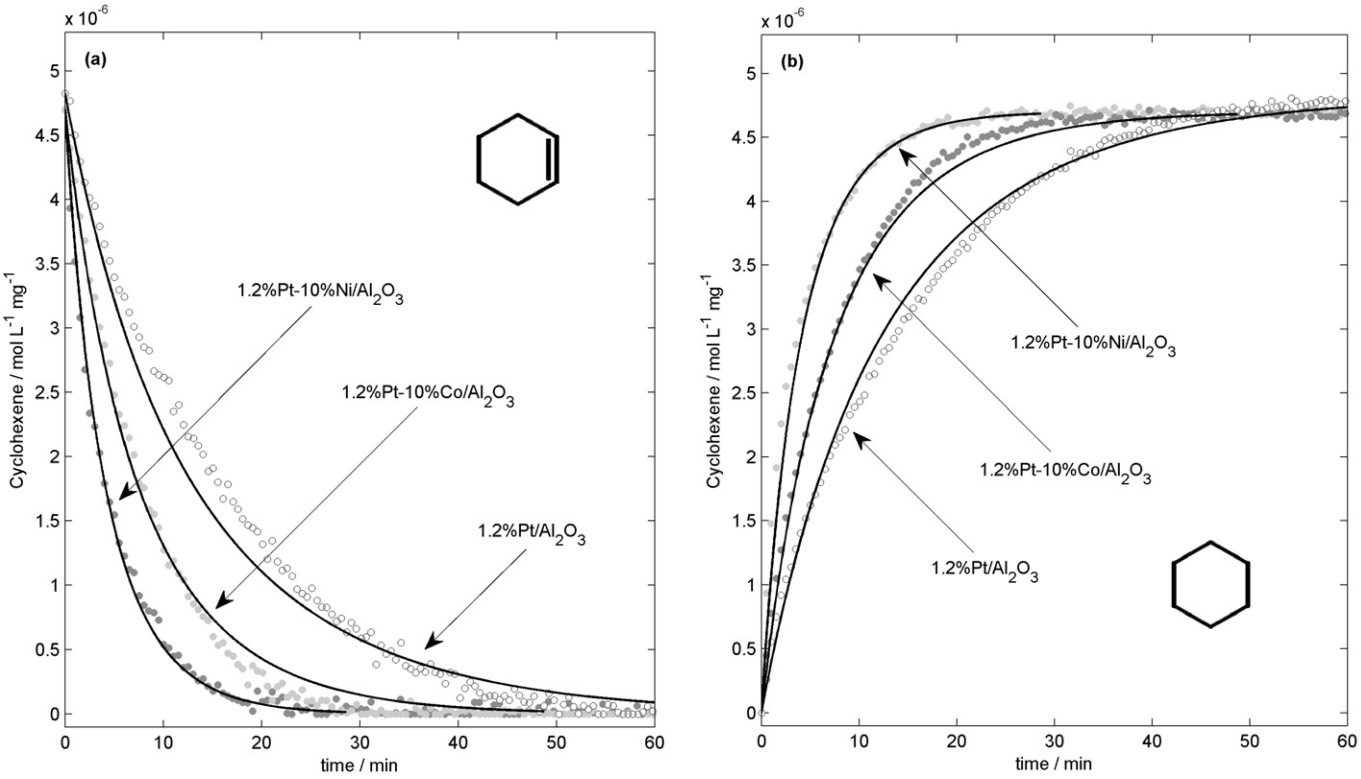

Fig. 6. The consumption of cyclohexene (a) and production of cyclohexane (b) during the hydrogenation of cyclohexene at 303 K. Also displayed are fits using Langmuir–Hinshelwood reaction kinetics (Eq. (1)).

Table 3
Langmuir–Hinshelwood rate coefficients for the hydrogenation of cyclohexene (Eq. (1)) and benzene (Eq. (2)) over different alumina-supported catalysts.

Catalyst	Cyclohexene k_1 (min^{-1})	Benzene k_{1-5} (min^{-1})
1.2%Pt/γ-Al_2O_3	1.74	1.33×10^4
1.2%Pt–10%Ni/γ-Al_2O_3	27.2	2.58×10^4
1.2%Pt–10%Co/γ-Al_2O_3	21.4	9.43×10^4

far more active for the hydrogenation of benzene when compared to the PtNi bimetallic and Pt monometallic catalysts. The difference in rates was modeled using a classic Langmuir–Hinshelwood equation proposed by Saeys and coworkers [54]. The model assumes the stepwise addition of six hydrogen atoms to the aromatic ring, with the addition of the fifth hydrogen being the rate-determining step. From these assumptions, the following equation was obtained for the rate of cyclohexane production from the hydrogenation of benzene:

$$r_{C_6H_{12}} = -r_{C_6H_6} = \frac{K_1K_2K_3K_4k_5K_BC_{C_6H_6}(K_{H_2}C_{H_2})^{5/2}}{(1+K_BC_{C_6H_6}+\sqrt{K_{H_2}C_{H_2}})^2} = \frac{k_{1-5}K_BC_{C_6H_6}(K_{H_2}C_{H_2})^{5/2}}{(1+K_BC_{C_6H_6}+\sqrt{K_{H_2}C_{H_2}})^2}. \quad (2)$$

Within the expression, K_1 through K_4 represent equilibrium constants for the first through fourth hydrogen additions and k_5 is the rate constant for the rate-determining fifth addition. These five constants were combined into a single rate constant (k_{1-5}) during the fitting procedure. Also included in the expression are the adsorption/desorption equilibrium constants, K_B and K_{H_2}, for molecular benzene and hydrogen, respectively. The same value for the hydrogen equilibrium constant was employed for the benzene modeling. The resulting fits obtained from the model are displayed in Fig. 7 overlaid on the experimental data. Table 3 summarizes the rate constants for the three catalysts for the hydrogenation of benzene, displaying the following trend in activity: 1.2%Pt–10%Co/γ-Al_2O_3 ≫ 1.2%Pt–10%Ni/γ-Al_2O_3 > 1.2%Pt/γ-Al_2O_3.

4. Discussion

Results presented above clearly demonstrate that the PtCo and PtNi bimetallic catalysts exhibit much higher hydrogenation activities than the corresponding monometallic catalysts. The enhanced activities could be attributed to the increased reducibility of Co(Ni) oxides by the addition of Pt, and more importantly, to the formation of the Pt–Co and Pt–Ni bimetallic alloys.

As indicated from the EXAFS results in Table 2, most of the Pt atoms in the bimetallic catalysts are surrounded by Co or Ni atoms to form the Pt–Co or Pt–Ni bimetallic bonds. In addition, the PtCo or PtNi bimetallic catalysts can be reduced much more easily than the monometallic Co or Ni catalysts, as demonstrated by the H_2-TPR results in Fig. 1. Consequently, the number of active sites is higher on the bimetallic catalysts, as supported by the H_2-chemisorption results in Table 1. For example, the H_2 uptake value for the 1.2%Pt–10%Co/γ-Al_2O_3 bimetallic catalyst is 30.6 μmols/g catalyst, which is higher than the sum of uptake from the two monometallic catalysts, 14.4 and 7.2 μmols/g catalyst for 10%Co/γ-Al_2O_3 and 1.2%Pt/γ-Al_2O_3, respectively. Similar increases in H_2 uptake are also observed for the other PtCo and PtNi bimetallic catalysts listed in Table 1. The increase in the number of active sites on the bimetallic catalysts should partially contribute to the enhanced hydrogenation activities as compared to the monometallic catalysts.

However, the increase in the surface active sites alone cannot fully account for the magnitude of increase in the hydrogenation activities. For example, as shown in Table 3, the hydrogenation rate of the 1.2%Pt–10%Co/γ-Al_2O_3 bimetallic catalyst is about 3 times higher than 1.2%Pt/γ-Al_2O_3 for cyclohexene hydrogenation and about 10 times higher for benzene hydrogenation,

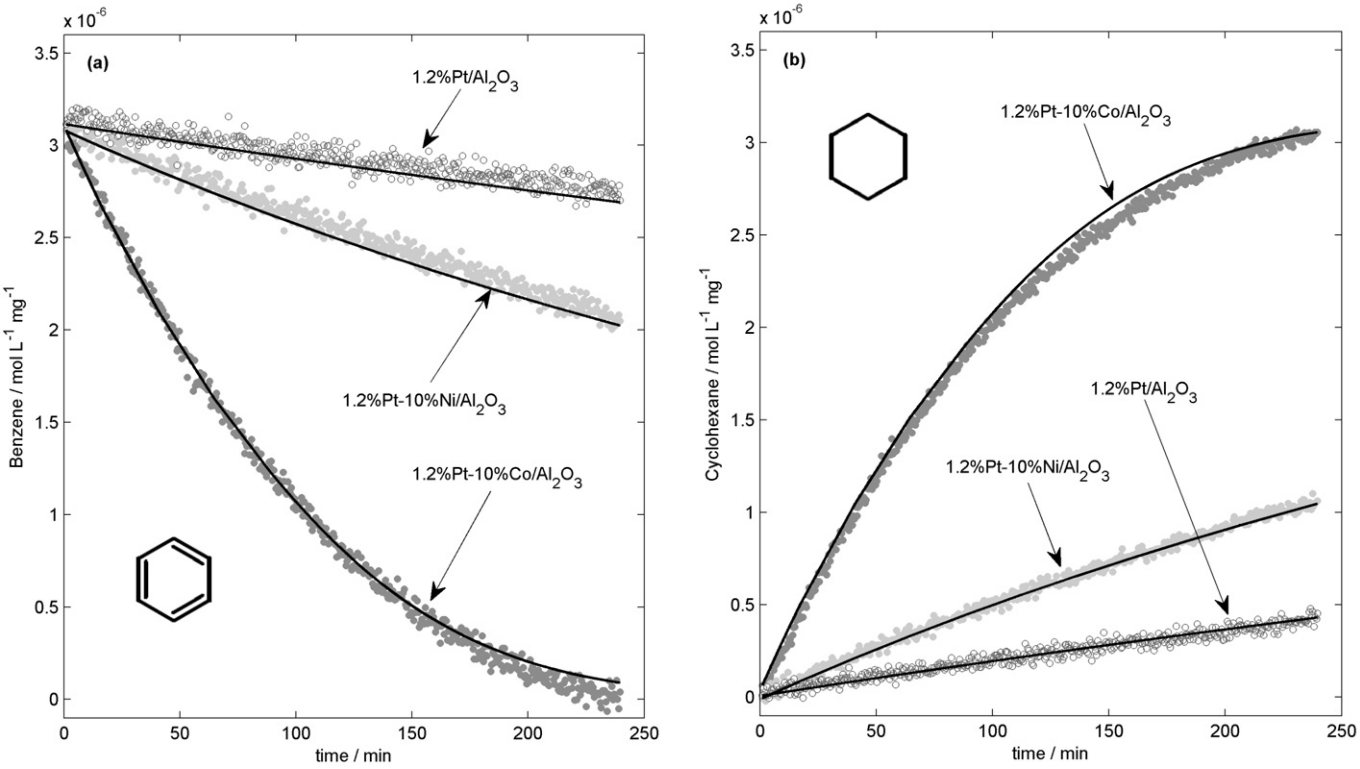

Fig. 7. The consumption of benzene (a) and production of cyclohexane (b) during the hydrogenation of benzene at 373 K. Also displayed are fits using Langmuir–Hinshelwood reaction kinetics (Eq. (2)).

with the latter being significantly higher than the increase in the number of surface sites from H_2 uptake. The enhanced hydrogenation activities are consistent with previous surface science studies [42,43] and density functional theory (DFT) modeling [40,47] of low-temperature hydrogenation of cyclohexene on Co/Pt(111) and Ni/Pt(111) bimetallic surfaces. In these studies bimetallic surfaces, with a monolayer of Co or Ni residing directly underneath surface Pt atoms, have shown hydrogenation activity that is significantly higher than that of the parent metal, Pt, Ni or Co surfaces. The higher hydrogenation activity has been attributed to the relatively weak binding energies of both atomic hydrogen and cyclohexene on the bimetallic surfaces, leading to a facile hydrogenation of cyclohexene [40,47].

As shown in both flow reactor (Figs. 3 and 4) and batch reactor (Figs. 6, 7 and Table 3) results, although both PtCo and PtNi catalysts exhibit higher hydrogenation activities than the parent metals, the two types of bimetallic catalysts demonstrate quite different catalytic performance between cyclohexene and benzene hydrogenation reactions. For cyclohexene hydrogenation, PtNi bimetallic catalysts show higher hydrogenation activity than PtCo. This difference can be attributed to two possible origins: (1) As compared in previous surface science and DFT studies [47], the Pt–Ni bimetallic surface exhibits higher hydrogenation activity than Pt–Co due to a difference in the binding energy of cyclohexene. (2) As compared in Table 1, the H_2 uptake is higher on the PtNi catalysts than PtCo, which should lead to a lower hydrogenation activity on PtCo assuming that the H_2 chemisorption capacity is directly related to the hydrogenation activity.

While the trend in the hydrogenation activity of cyclohexene, PtNi > PtCo > Pt, is consistent with previous surface science experiments and DFT modeling on the corresponding single crystal surfaces, the significantly higher hydrogenation activity of benzene over the PtCo catalysts suggests unique hydrogenation properties. For benzene hydrogenation, the PtCo bimetallic catalysts exhibit much higher activity than PtNi, as illustrated in the rate constants from batch reactor studies and the apparent activation energies from flow reactor studies. As compared in Fig. 7 and Table 3, the rate constant for the conversion of benzene over 1.2%Pt–10%Co/γ-Al_2O_3 is significantly higher than over 1.2%Pt–10%Ni/γ-Al_2O_3. This trend is consistent with the flow reactor results of benzene conversion in Fig. 4 and with the estimation of the apparent activation energy in Fig. 5, where the value is estimated to be 33.7 kJ/mol over 1.2%Pt–10%Co/γ-Al_2O_3 and 56.8 kJ/mol over 1.2%Pt–10%Ni/γ-Al_2O_3. For both monometallic and bimetallic catalysts studied here, Co-based catalysts show higher benzene hydrogenation activity than the corresponding Ni-based counterparts, suggesting that Co is an important metal component for benzene hydrogenation at low temperatures. However, the supported monometallic Co catalyst alone is not a good catalyst for benzene hydrogenation because Co metals do not adsorb and dissociate hydrogen effectively, as supported by the H_2 chemisorption results that Co-based catalysts have smaller hydrogen adsorption capacity than Ni-based catalysts (Table 1).

Although the exact origins are unknown regarding the synergistic effect on benzene hydrogenation by alloying Pt and Co, one could argue that some of the following factors are contributing to the high benzene hydrogenation activities over the PtCo bimetallic catalysts: (1) The presence of Pt facilitates the reduction of Co_3O_4 and leads to an increase in the number of metal sites. (2) Because Pt is an efficient catalyst for hydrogen adsorption and dissociation, it could provide atomic hydrogen to the Co metal sites for hydrogenation through the spillover effect. (3) A closer inspection of the results in Fig. 5 suggests that Co is an active hydrogenation catalyst. For example, the apparent activation barriers over the 10%Co/Al_2O_3 and 1.2%Pt–10%Co/Al_2O_3 are essentially identical, at 33.7 and 33.8 kJ/mol, respectively. Therefore, the role of Pt appears to be to keep Co in its reduced state and may also provide sites for the dissociation of H_2. Although more detailed experimental and theoretical studies are needed to understand the origins, it is clear that γ-Al_2O_3 supported PtCo bimetallic catalysts exhibit

high activities for benzene hydrogenation at relatively low temperatures.

5. Conclusions

Supported PtCo, PtNi bimetallic and Co, Ni, Pt monometallic catalysts on γ-Al_2O_3 have been prepared by simple impregnation method and evaluated using flow and batch reactors for benzene and cyclohexene hydrogenation at low temperatures and atmospheric pressure. The results showed that supported PtCo bimetallic catalysts exhibited the highest activity among all as-prepared catalysts in benzene hydrogenation, which mostly attributed to the Pt–Co bimetallic formation. The PtNi bimetallic catalysts, while possessing high activity in cyclohexene hydrogenation, exhibited much lower activity than PtCo catalysts in benzene hydrogenation. Overall, the PtCo and PtNi bimetallic catalysts showed higher hydrogenation activities than the corresponding monometallic catalysts and exhibited distinct hydrogenation activities for benzene and cyclohexene, supporting the argument from previous surface science and theoretical predictions that these bimetallic catalysts would have unique catalytic properties.

Acknowledgments

The work was supported by the National Science Foundation of China (20440420577) and the Major State Basic Research Development Program (Grant No. G2006CB806100). The authors from the University of Delaware acknowledge financial support from the Basic Energy Sciences of the United States Department of Energy (DOE/BES Grant No. DE-FG02-00ER15104). Use of the National Synchrotron Light Source, Brookhaven National Laboratory, for the EXAFS experiments was supported by the United States Department of Energy (DOE/BES Grant No. DE-FG02-05ER15688).

References

[1] J.-F. Le Page, Applied Heterogeneous Catalysis: Design, Manufacture, Use of Solid Catalysts, Technip, Paris, 1987, p. 291.
[2] A. Stanislaus, B.H. Cooper, Catal. Rev. Sci. Eng. 36 (1994) 75.
[3] R.Z.C. van Meerten, J.W.E. Coenen, J. Catal. 37 (1975) 37.
[4] R.Z.C. van Meerten, A.C.M. Verhaak, J.W.E. Coenen, J. Catal. 44 (1976) 217.
[5] H.A. Franco, M.J. Phillips, J. Catal. 63 (1980) 346.
[6] A. Jasik, R. Wojcieszak, S. Monteverdi, M. Ziolek, M.M. Bettahar, J. Mol. Catal. A Chem. 242 (2005) 81.
[7] A. Louloudi, J. Michalopoulos, N.H. Gangas, N. Papayannakos, Appl. Catal. A 242 (2003) 41.
[8] A. Louloudi, N. Papayannakos, Appl. Catal. A 175 (1998) 21.
[9] A. Louloudi, N. Papayannakos, Appl. Catal. A 204 (2000) 167.
[10] G. Marcelin, R.F. Vogel, H.E. Swift, J. Catal. 98 (1986) 64.
[11] F. Mittendorfer, J. Hafner, J. Phys. Chem. B 106 (2002) 13299.
[12] R. Molina, G. Poncelet, J. Catal. 199 (2001) 162.
[13] S. Toppinen, T.K. Rantakyla, T. Salmi, J. Aittamaa, Ind. Eng. Chem. Res. 35 (1996) 1824.
[14] R. Badilla-Ohlbaum, H.J. Neuburg, W.F. Graydon, M.J. Phillips, J. Catal. 47 (1977) 273.
[15] M.I. Phillips, P.H. Emmett, J. Catal. 101 (1986) 268.
[16] K.J. Yoon, M.A. Vannice, J. Catal. 82 (1983) 457.
[17] J.M. Basset, G. Dalmai-Imelik, M. Primet, R. Mutin, J. Catal. 37 (1975) 22.
[18] S.D. Lin, M.A. Vannice, J. Catal. 143 (1993) 539.
[19] P. Chou, M.A. Vannice, J. Catal. 107 (1987) 129.
[20] P. Chou, M.A. Vanice, J. Catal. 107 (1987) 140.
[21] C. Milone, G. Neri, A. Donato, M.G. Musolino, J. Catal. 159 (1996) 253.
[22] L. Ronchin, L. Toniolo, Catal. Today 66 (2001) 363.
[23] J.Q. Wang, P.J. Guo, S.R. Yan, M.H. Qiao, H.X. Li, K.N. Fan, J. Mol. Catal. A Chem. 222 (2004) 229.
[24] S.-W. Ho, J.M. Cruz, M. Houalla, D.M. Hercules, J. Catal. 135 (1992) 173.
[25] J.M. Jablonski, D. Potocznapetru, J. Okal, L. Krajczyk, React. Kinet. Catal. Lett. 54 (1995) 15.
[26] W.F. Taylor, J. Catal. 9 (1967) 99.
[27] W.F. Taylor, H.K. Staffin, J. Phys. Chem. 71 (1967) 3314.
[28] L.J. Simon, P.J. Kooyman, J.G. van Ommen, J.A. Lercher, Appl. Catal. A 252 (2003) 283.
[29] P. Tétényi, V. Galsan, Appl. Catal. A 229 (2002) 181.
[30] M.H. Qiao, S.H. Xie, W.L. Dai, J.F. Deng, Catal. Lett. 71 (2001) 187.
[31] X.D. Mu, J.Q. Meng, Z.C. Li, Y. Kou, J. Am. Chem. Soc. Commun. 127 (2005) 9694.
[32] B. Jongsomjit, J. Panpranot, J.G. Goodwin, J. Catal. 215 (2003) 66.
[33] G. Jacobs, T.K. Das, P.M. Patterson, L. Sanchez, B.H. Davis, Appl. Catal. A 247 (2003) 335.
[34] J.H. Sinfelt, Accounts Chem. Res. 10 (1977) 15.
[35] J.H. Sinfelt, Bimetallic Catalysts: Discoveries, Concepts, and Applications, Wiley, New York, 1983.
[36] J.A. Rodriguez, Surf. Sci. Rep. 24 (1996) 225.
[37] B. Hammer, J.K. Nørskov, Surf. Sci. 343 (1995) 211.
[38] D.W. Goodman, J. Phys. Chem. 100 (1996) 13090.
[39] V. Pallassana, M. Neurock, J. Catal. 191 (2000) 301.
[40] J.G. Chen, C.A. Menning, M.B. Zellner, Surf. Sci. Rep. 63 (2008) 201.
[41] J. Greeley, M. Mavrikakis, Nat. Mater. 3 (2004) 810.
[42] H.H. Hwu, J. Eng Jr., J.G. Chen, J. Am. Chem. Soc. 124 (2002) 702.
[43] N.A. Khan, L.E. Murillo, J.G. Chen, J. Phys. Chem. B 108 (2004) 15748.
[44] J.R. Kitchin, N.A. Khan, M.A. Barteau, J.G. Chen, B. Yakshinksiy, T.E. Madey, Surf. Sci. 544 (2003) 295.
[45] J.R. Kitchin, J.K. Nørskov, M.A. Barteau, J.G. Chen, Phys. Rev. Lett. 93 (2004) 156801.
[46] L.E. Murillo, A.M. Goda, J.G. Chen, J. Am. Chem. Soc. 129 (2007) 7101.
[47] M.P. Humbert, L.E. Murillo, J.G. Chen, Chem. Phys. Chem. 9 (2008) 1262.
[48] Y. Shu, L.E. Murillo, J.P. Bosco, W. Huang, A.I. Frenkel, J.G. Chen, Appl. Catal. A 339 (2008) 169.
[49] M. Newville, J. Synchrotron Radiat. 8 (2001) 96.
[50] B. Ravel, M. Newville, J. Synchrotron Radiat. 12 (2005) 537.
[51] NIST, Chemistry WebBook.
[52] E.V. Steen, G.S. Sewell, R.A. Makhothe, C. Mickelethwaite, H. Manstein, M. de Lange, C.T. O'Connor, J. Catal. 162 (1996) 220.
[53] A.B. Mhadeshwar, J.R. Kitchin, M.A. Barteau, D.G. Vlachos, Catal. Lett. 96 (2004) 13.
[54] M. Saeys, M.-F. Reyniers, J.W. Thybaut, M. Neurock, G.B. Marin, J. Catal. 236 (2005) 129.